Fourier-transform method of fringe-pattern analysis for computer-based topography and interferometry

Mitsuo Takeda, Hideki Ina* and Seiji Kobayashi

University of Electrocommunications, 1-5-1, Chofugaoka, Chofu, Tokyo, 182, Japan

Received May 7, 1981; revised manuscript received August 27, 1981

A fast-Fourier-transform method of topography and interferometry is proposed. By computer processing of a noncontour type of fringe pattern, automatic discrimination is achieved between elevation and depression of the object or wave-front form, which has not been possible by the fringe-contour-generation techniques. The method has advantages over moiré topography and conventional fringe-contour interferometry in both accuracy and sensitivity. Unlike fringe-scanning techniques, the method is easy to apply because it uses no moving components.

INTRODUCTION

In various optical measurements, we find a fringe pattern of the form

$$g(x,y) = a(x,y) + b(x,y)\cos[2\pi f_0 x + \phi(x,y)], \quad (1)$$

where the phase $\phi(x,y)$ contains the desired information and $a(x,y)$ and $b(x,y)$ represent unwanted irradiance variations arising from the nonuniform light reflection or transmission by a test object; in most cases $a(x,y)$, $b(x,y)$ and $\phi(x,y)$ vary slowly compared with the variation introduced by the spatial-carrier frequency f_0.

The conventional technique has been to extract the phase information by generating a fringe-contour map of the phase distribution. In interferometry, for which Eq. (1) represents the interference fringes of tilted wave fronts, the tilt is set to zero to obtain a fringe pattern of the form

$$g_0(x,y) = a(x,y) + b(x,y)\cos[\phi(x,y)], \quad (2)$$

which gives a contour map of $\phi(x,y)$ with a contour interval 2π. In the case of moiré topography,[1] for which Eq. (1) represents a deformed grating image formed on an object surface, another grating of the same spatial frequency is superposed to generate a moiré pattern that has almost the same form as Eq. (2) except that it involves other high-frequency terms that are averaged out in observation. Although these techniques provide us with a direct means to display a contour map of the distribution of the quantity to be measured, they have following drawbacks: (1) The sign of the phase cannot be determined, so that one cannot distinguish between depression and elevation from a given contour map. (2) The sensitivity is fixed at 2π because phase variations of less than 2π create no contour fringes. (3) Accuracy is limited by the unwanted variations $a(x, y)$ and $b(x, y)$, particularly in the case of broad-contour fringes. Fringe-scanning techniques[2] have been proposed to solve these problems, but they require moving components, such as a moving mirror mounted on a translator, which must be driven with great precision and stability.

We propose a new technique that can solve all these problems by a simple Fourier-spectrum analysis of a noncontour type of fringe pattern, as given in Eq. (1).

PRINCIPLE AND OPERATION

First, a noncontour type of fringe pattern of the form given in Eq. (1) is put into a computer by an image-sensing device that has enough resolution to satisfy the sampling-theory requirement, particularly in the x direction. The input fringe pattern is rewritten in the following form for convenience of explanation:

$$g(x,y) = a(x,y) + c(x,y)\exp(2\pi i f_0 x) + c^*(x,y)\exp(-2\pi i f_0 x), \quad (3)$$

with

$$c(x,y) = (\tfrac{1}{2})b(x,y)\exp[i\phi(x,y)], \quad (4)$$

where $*$ denotes a complex conjugate.

Next, Eq. (3) is Fourier transformed with respect to x by the use of a fast-Fourier-transform (FFT) algorithm, which gives

$$G(\mathrm{f},\mathrm{y}) = A(f,y) + C(f - f_0, y) + C^*(f + f_0, y), \quad (5)$$

where the capital letters denote the Fourier spectra and f is the spatial frequency in the x direction. Since the spatial variations of $a(x, y)$, $b(x, y)$, and $\phi(x, y)$ are slow compared with the spatial frequency f_0, the Fourier spectra in Eq. (5) are separated by the carrier frequency f_0, as is shown schematically in Fig. 1(A).[3] We make use of either of the two spectra on the carrier, say $C(f - f_0, y)$, and translate it by f_0 on the frequency axis toward the origin to obtain $C(f, y)$, as is shown in Fig. 1(B). Note that the unwanted background variation $a(x, y)$ has been filtered out in this stage. Again using the FFT algorithm, we compute the inverse Fourier transform of $C(f, y)$ with respect to f and obtain $c(x, y)$, defined by Eq. (4). Then we calculate a complex logarithm of Eq. (4):

$$\log[c(x,y)] = \log[(\tfrac{1}{2})b(x,y)] + i\phi(x,y). \quad (6)$$

Now we have the phase $\phi(x, y)$ in the imaginary part completely separated from the unwanted amplitude variation $b(x, y)$ in the real part. The phase so obtained is indeterminate to a factor of 2π. In most cases, a computer-generated function subroutine gives a principal value ranging from $-\pi$ to π, as, for example, is shown in Fig. 2(A). These discontinuities can be corrected by the following algorithm. We determine

0030-3941/82/010156-05$01.00

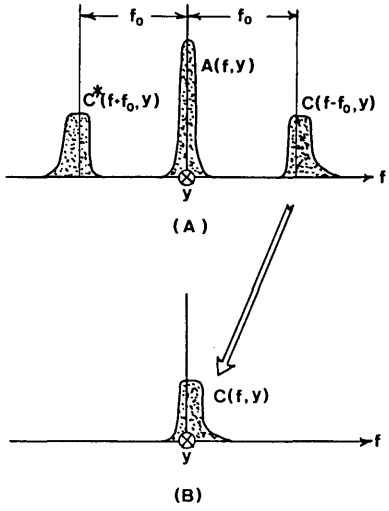

Fig. 1. (A) Separated Fourier spectra of a noncontour type of fringe pattern; (B) single spectrum selected and translated to the origin. The y axis is normal to the figure.

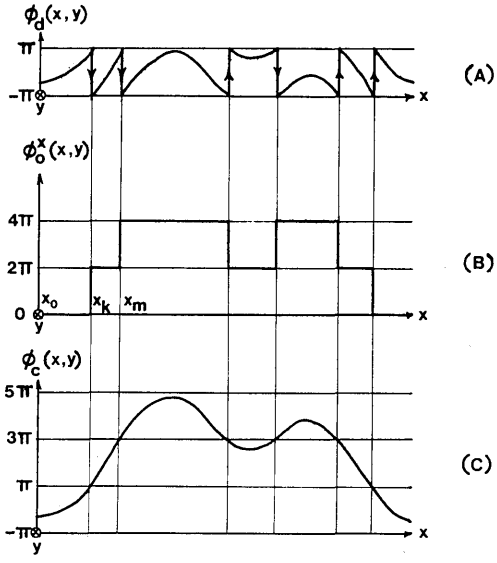

Fig. 2. (A) Example of a phase distribution having discontinuities that are due to the principal-value calculation; (B) offset phase distribution for correcting the discontinuities in (A); (C) continued profile of the phase distribution. The y axis is normal to the figure.

an offset phase distribution $\phi_o(x, y)$ that should be added to the discontinuous phase distribution $\phi_d(x, y)$ to convert it to a continuous distribution $\phi_c(x, y)$:

$$\phi_c(x, y) = \phi_d(x, y) + \phi_o(x, y). \quad (7)$$

The first step in making this determination is to compute the phase difference

$$\Delta\phi_d(x_i, y) = \phi_d(x_i, y) - \phi_d(x_{i-1}, y)$$

between the ith sample point and the point preceding it, with the suffix i running from 1 to N to cover all the sample points. Since the variation of the phase is slow compared with the sampling interval, the absolute value of the phase difference $|\Delta\phi_d(x_i, y)|$ is much less than 2π at points where the phase distribution is continuous. But it becomes almost 2π at points where the 2π phase jump occurs. Hence, by setting an appropriate criterion for the absolute phase difference, say $0.9 \times 2\pi$, we can specify all the points at which the 2π phase jump takes place and also the direction of each phase jump, positive or negative, which is defined as corresponding to the sign of $\Delta\phi_d(x_i, y)$. The second step is to determine the offset phase at each sample point sequentially, starting from the point $x_0 = 0$. Since only a relative phase distribution needs to be determined, we initially set $\phi_o{}^x(x_0, y) = 0$.[4] Then we set $\phi_o{}^x(x_i, y) = \phi_o{}^x(x_0, y)$ for $i = 1, 2, 3, \ldots, k-1$ until the first phase jump is detected at the kth sample point. If the direction of the phase jump is positive (as marked by ↑ in the figure), we set $\phi_o{}^x(x_k, y) = \phi_o{}^x(x_{k-1}, y) - 2\pi$, and if it is negative (as marked by ↓), we set $\phi_o{}^x(x_k, y) = \phi_o{}^x(x_{k-1}, y) + 2\pi$. Again, we start to set $\phi_o{}^x(x_i, y) = \phi_o{}^x(x_k, y)$ for $i = k+1, i = k+2, \ldots, i = m-1$, until the next phase jump occurs at the mth sample point, where we perform the same 2π addition or subtraction as at the kth sample point, with k now being replaced with m. Repeating this procedure of 2π phase addition or subtraction at the points of phase jump, we can determine the offset phase distribution, as shown in Fig. 2(B), the addition of which to $\phi_d(x, y)$ gives a continuous phase distribution $\phi_c(x, y)$, as is shown in Fig. 2(C). In the case of measurement over a full two-dimensional plane, a further phase-continuation operation in the y direction is necessary because we initially set $\phi_o{}^x(x_0, y) = 0$ for all y without respect to the phase distribution in the y direction. It is sufficient to determine an additional offset phase distribution in the y direction, $\phi_o{}^y(x, y)$, on only one line along the y axis, say, on the line through the point $x = x_L$, L being arbitrary. This can be done by the same procedure as was described for the x direction, with the initial value now being set at $\phi_o{}^y(x_L, y_0) = 0$. The two-dimensional offset phase distribution is then given by

$$\phi_o(x, y) = \phi_o{}^x(x, y) - \phi_o{}^x(x_L, y) + \phi_o{}^x(x_L, y). \quad (8)$$

In Eq. (8), $\phi_o{}^x(x, y) - \phi_o{}^x(x_L, y)$ represents the difference of the offset phase between the points (x, y) and (x_L, y), and $\phi_o{}^y(x_L, y)$ that between points (x_L, y) and (x_L, y_0), so that $\phi_o(x, y)$ gives a relative offset phase distribution defined as the difference from the initial value at (x_L, y_0).

EXPERIMENTS

The validity of the proposed method was examined in experiments using a Michelson interferometer with a He–Ne laser source. Figure 3 shows[5] an example of the interference fringes of tilted wave fronts put into a microcomputer (Digital LSI-11/2) by a solid-state line-image sensor (Reticon RL1024H) with 1024 photodiode elements separated from one another by 15 μm; a sensor of this type is particularly suited for our purpose because it has high resolution and accuracy in the position of elements and a number of elements that is convenient for an FFT algorithm. Note the presence in Fig. 3 of unwanted irradiance variations corresponding to $a(x, y)$ and $b(x, y)$ in Eq. (1).

Before computing by the FFT algorithm, we weighted the data by the multiplication of a hanning window, as is shown in Fig. 4, to eliminate the influence of the discontinuity of the data at the both ends. Figure 5 shows the computed spatial-frequency spectra corresponding to Eq. (5); the spectra are separated by the carrier frequency $f_0 = 3$ lines/mm. Only

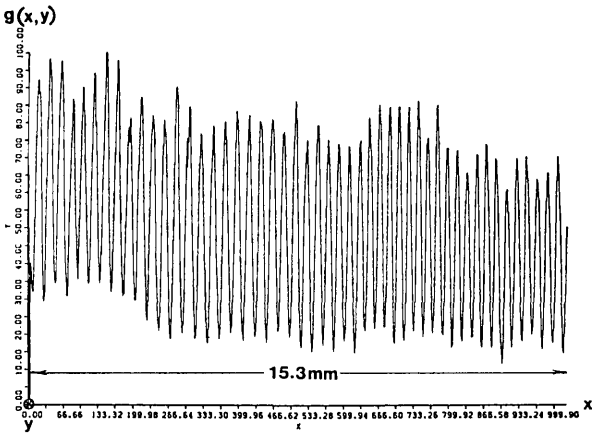

Fig. 3. Intensity distribution of the interference fringes of tilted wave fronts taken into the microcomputer.

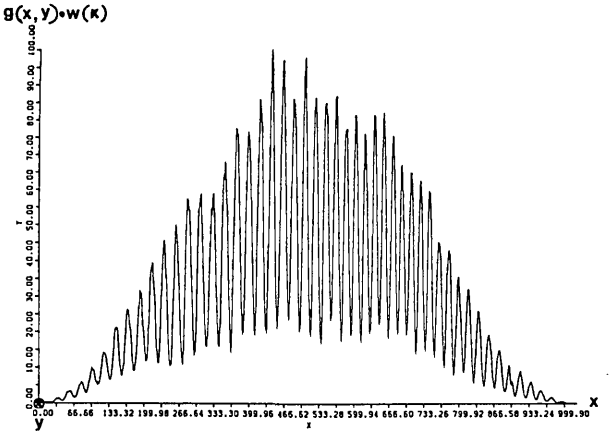

Fig. 4. Distribution of the interference fringes weighted by a hanning window $w(x) = 1 - \cos(2\pi x/D)$, where D is the range of the measurement (15.3 mm).

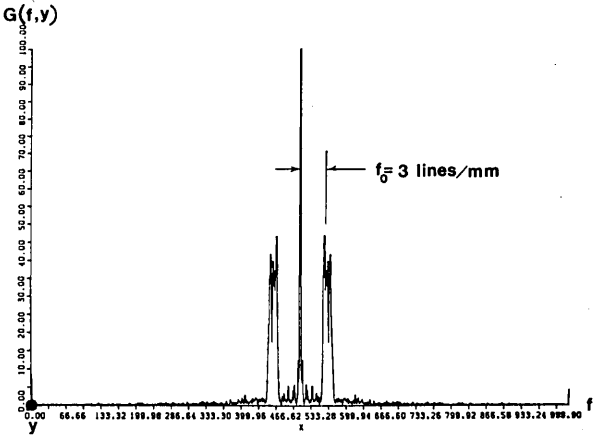

Fig. 5. Computed spatial-frequency spectra. The zero-frequency spectrum is clipped to enhance the detail of the spectra on the carriers.

one spectral sideband was selected and shifted by f_0 toward the origin, and its inverse Fourier transform was computed again by the FFT algorithm to obtain $c(x, y)$ in Eq. (4). The complex logarithm of $c(x, y)$ was then computed; the discontinuous phase distribution $\phi_d(x, y)$ obtained from the imaginary part is shown in Fig. 6(b). Figure 6(a) shows conventional contour fringes generated by inserting a heat source in one of the arms of the tilt-free interferometer. The measurement shown in Fig. 6(b) was made over a range of the line segment marked by ⊢⊣ in the picture. Note that in this ex-

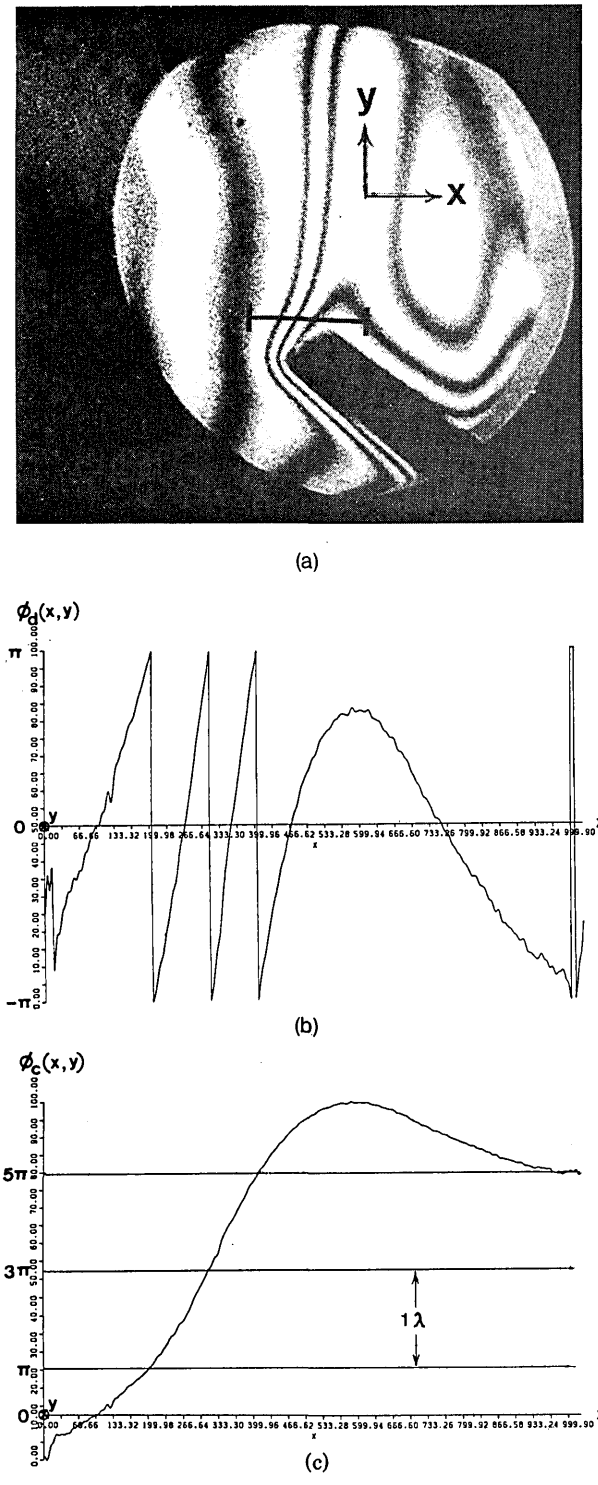

Fig. 6. (a) Conventional contour fringes showing the index distribution around the heat source; (b) discontinuous phase distribution obtained by measurement over a range of the line segment marked by ⊢⊣ in (a); (c) corrected continuous phase distributions representing a complete profile of the phase value over the range marked by ⊢⊣ in (a).

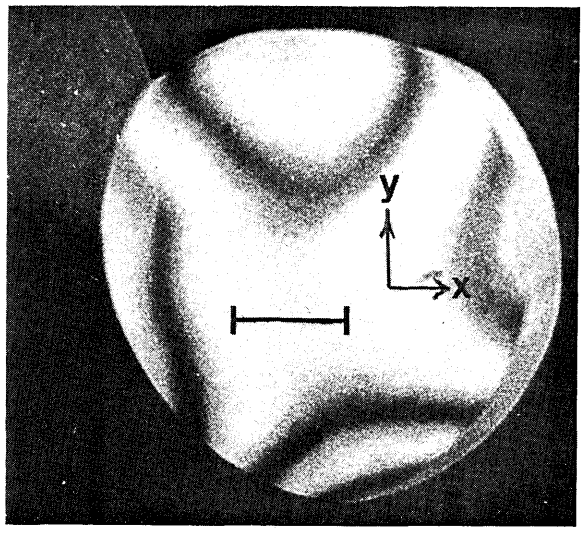

(a)

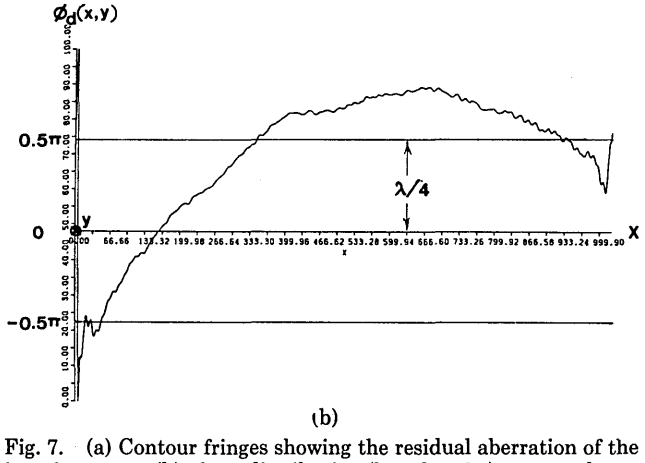

(b)

Fig. 7. (a) Contour fringes showing the residual aberration of the interferometer; (b) phase distribution (less than 2π) measured over a range of the line segment marked by ⊢⊣ in (a).

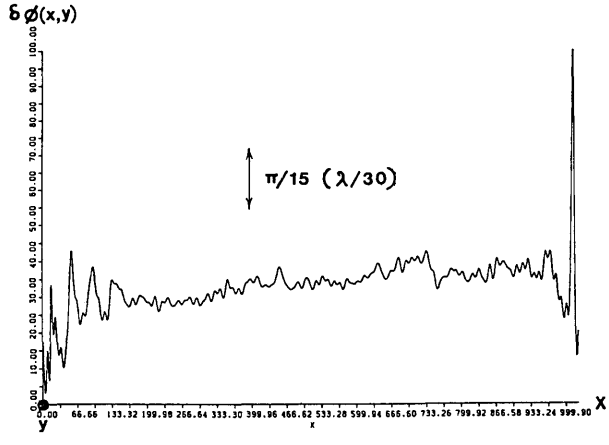

Fig. 8. Effect of noise on the fluctuation of the measured phase distribution.

ample the position of 2π phase jumps coincides with that of dark fringes. The discontinuous distribution in Fig. 6(b) was corrected by adding an offset phase, as described in the preceding section. Figure 6(c) shows the continuous distribution, which gives a complete profile of the phase measured over the range of the line segment marked by ⊢⊣ in Fig. 6(a). Note that the profile can be determined uniquely without ambiguity about the distinction between elevation and depression of the wave front form.

To demonstrate the sensitivity of the measurement, one more example is given in Fig. 7. Figure 7(a) shows contour-type fringes obtained when the heat source was removed; it represents a residual aberration of the interferometer. Here again, the measurement was made over a range of the line segment marked by ⊢⊣ in the picture, and the result is shown in Fig. 7(b). Note that a phase distribution of less than 2π is clearly detected by the proposed method, whereas it cannot be observed in the picture of the contour-type fringes. The residual aberration of the interferometer is stored in the memory of the computer and is subtracted from the measurement data to correct the error it has caused. This permits the use of optical elements of rather low quality even for the measurement of phase distributions less than 2π.

To see the effect of noise, the same object was measured twice with a 1-min interval between measurements; the difference in the results was computed and is shown in Fig. 8. As can be seen in the figure, the fluctuation that is due to noise is less than $\lambda/30$, except at the ends of the measurement range. The increase of errors at the ends is due to the use of the hanning window. Because the fringe amplitude becomes zero in these regions, as is seen in Fig. 4, the determination of phase becomes quite sensitive to noise.

CONCLUSION

A Fourier-transform method of computer-based fringe-pattern analysis has been proposed and verified by experiments. The method has the sensitivity for detecting phase variations of less than 2π and can be applied to subwavelength interferometry without a fringe-scanning process. The accuracy has been improved by the complete separation of the phase from other unwanted irradiance variations. By use of this method, clear distinction can be made between elevation and depression, even from a single fringe pattern. When the method is applied to topography, it permits fully automatic measurement without man–machine communication, as is needed for the fringe-order assignment in computer-aided moiré topography; further, because only one selected spectrum is used, the method has the additional merit that the measurement is not disturbed by higher-order harmonics, which are included in a nonsinusoidal grating pattern and give rise to spurious moiré fringes in the case of moiré topography.

The authors thank T. Yatagai of the Institute of Physical and Chemical Research for helpful discussions and H. Sato and T. Mimaki of the University of Electrocommunications for their interest and encouragement.

* Present address, Optical Products Development Division, Canon Inc., 53, Imaikamicho, Nakahara, Kawasaki, Kanagawa, 211, Japan.

REFERENCES

1. See, for example, D. M. Meadows, W. O. Johnson, and J. B. Allen, "Generation of surface contours by moiré patterns," Appl. Opt. 9, 942–947 (1970); H. Takasaki, "Moiré topography," Appl. Opt.

9, 1467–1472 (1970). Although these papers describe methods that use a shadow of a grating, our proposed method applies to a projected grating image as in projection-type moiré topography; for a discussion of projection-type moiré topography, see, for example, M. Idesawa, T. Yatagai, and T. Soma, "Scanning moiré method and automatic measurement of 3-D shape," Appl. Opt. **16**, 2152–2162 (1977).

2. See, for example, J. H. Bruning, "Fringe scanning interferometers," in *Optical Shop Testing*, D. Malacara, ed. (Wiley, New York, 1978), pp. 409–437.

3. In all figures, the variation in the y direction is not illustrated because it is not necessary for the explanation of the principle.
4. The superscript x denotes that $\phi_o{}^x(x, y)$ is an offset phase for correcting discontinuities in the x direction along a line for which y is fixed; the same is denoted by the superscript y for the y direction. The offset phase without a superscript means that discontinuities can be corrected by it in both x and y directions.
5. In all figures, note only the scales indicated by large letters and ignore the fine letters and scales on the axes drawn by the graphic plotter subroutine.